Available online at www.sciencedirect.com
SCIENCE DIRECT
Journal of Sound and Vibration 295 (2006) 571–583
JOURNAL OF SOUND AND VIBRATION
www.elsevier.com/locate/jsvi

Dynamic stability of ring-based angular rate sensors

Samuel F. Asokanthan*, Jihyun Cho

Department of Mechanical and Materials Engineering, The University of Western Ontario, London, Ont., Canada N6A 5B9

Received 8 March 2005; received in revised form 27 December 2005; accepted 6 January 2006
Available online 27 April 2006

Abstract

Dynamic stability of a rotating ring subjected to harmonic perturbations in input angular rate is examined using an asymptotic approach. The governing equations that represent the transverse and tangential in-plane motion of the ring are derived via Hamilton's principle. The equations of motion, after discretization and suitable linearization, represent a two-degree-of-freedom time-varying linear gyroscopic system. Such a system can exhibit instability behaviour characterized by exponential growth in response amplitudes. Employing the method of averaging, conditions for instability are obtained in closed-form. Instability boundaries for the ring in the excitation intensity-frequency space are then established for small excitation amplitudes. In addition, effects of damping, input angular rate variations, and imperfection due to the ring asymmetry are discussed.

1. Introduction

Conventional angular rate sensors such as mechanical and fibre-optic/laser gyroscopes have been traditionally used in applications where emphasis is placed on precise measurement of angular motion or angular rate of a rotating body. These systems typically lead to large, expensive and mechanically/electrically sophisticated packages [1]. Thus, an alternative technology using vibrating structures to provide gyroscopic torque from Coriolis acceleration had received noticeable attention owing to the potential for mass production of these devices via micromachining processes. In this class of devices, elements such as beams, tuning forks, spring-mass, and thin rings have been used to represent the vibratory structural element. In recent years, ring-type structures have gained much acceptance due to inherent advantages such as minimal drift to temperature fluctuation, high sensitivity to rotation, and less sensitivity to environment vibrations [2,3]. In practice, when these devices are mounted on a rotating body, they can be influenced by a harmonic perturbation of small intensity due to fluctuations in the system itself and/or from the surrounding environment. The purpose of the present study is to investigate the stability behaviour, taking this fluctuation into consideration.

A significant number of studies on dynamics of rotating rings have been performed in the recent past. Huang and Soedel [4] studied the in-plane vibrations of rotating rings, and Eley et al. [5] performed a study on the effects of Coriolis coupling between the in-plane and out-of-plane motions. Stability investigations on

*Corresponding author. Tel.: +1 519 661 2111x88907; fax: +1 519 661 3020.
E-mail addresses: sasokanthan@eng.uwo.ca (S.F. Asokanthan), jcho23@uwo.ca (J. Cho).

0022-460X/$ - see front matter © 2006 Elsevier Ltd. All rights reserved.
doi:10.1016/j.jsv.2006.01.028

different forms of rotating mechanical systems have also received notable attention. Stability analysis of a linear gyroscopic system that represents the motion of a rotating beam was performed by Kammer and Schlack [6]. In this paper, effects of periodic perturbation in the spin rate on the stability behaviour of the system were studied by employing the Krylov–Bogoliubov–Mitropolsky (KBM) method, while Van Doorn and Asokanthan [7] used the method of averaging for studying the stability of a rotating dual-spin spacecraft. Natsiavas [8] investigated the stability of rotating thin circular rings subjected to parametric angular velocity excitation. In this study, nonlinear effects were included, and instability regions for the case of combination parametric resonance were established via the method of multiple time scales.

In the present study, an approximate form of the equations of motion is first obtained from a rotating ring model developed by Huang and Soedel [4] assuming that the ring is perfectly symmetric. In practice, however, the ring may not be perfectly symmetric, and the asymmetry causes differences in either or both the mass and stiffness of the ring [5]. Hence, for more accurate predictions of dynamics and stability characteristics, inclusion of the above effects is warranted. Although both mass and stiffness asymmetries are caused by asymmetry of the ring, both terms affect the non-rotating ring natural frequencies. In order to demonstrate the effect of ring asymmetry, inclusion of one of these terms is adequate. Hence, in the present study, only a difference in the mass is assumed for simplicity. Also, in the present study, the input angular rate is considered time varying, and as a result the centrifugal terms appear explicitly in the approximated model. Closed-form stability conditions are obtained via the Method of Averaging, and these conditions when plotted in a suitable parameter space give much insight on the stability behaviour. Instability regions in the excitation intensity-frequency space are established and discussed for varying parameter values of damping and input angular rate with the effects due to ring asymmetry included. It is envisaged that the results from the present study may be used for improving the design of this class of devices, so that they can be used in applications that demand high accuracy and sensitivity.

2. Equations of motion

The ring used for the present study is assumed to possess isotropic and homogeneous material properties, and the transverse shear deformation effects are considered negligible based on the Bernoulli–Euler theory [9]. Fig. 1 illustrates the ring supported internally with eight springs. The support springs are considered to possess significantly low stiffness and hence assumed not to have significant effects on the ring dynamics.

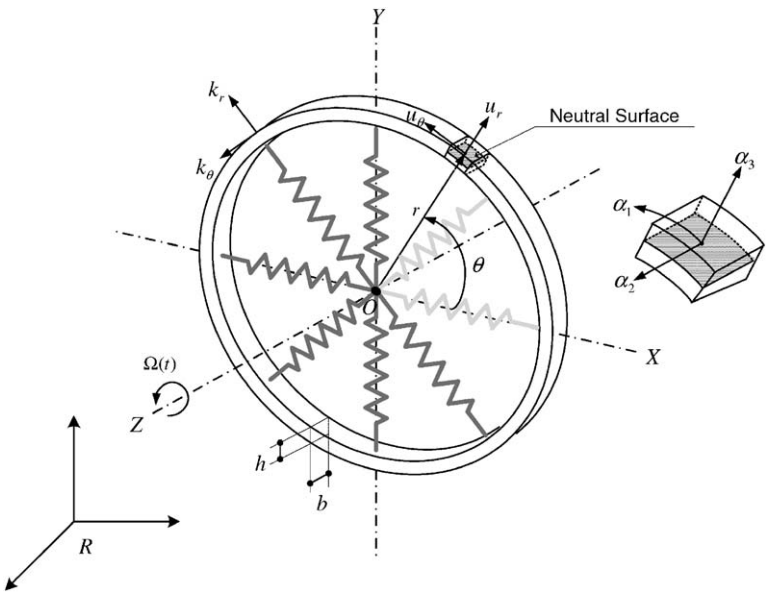

Fig. 1. Schematic of rotating ring with support springs.

A body fixed frame, $X-Y-Z$, has been used for representing the angular motion of the ring with respect to the inertial frame R, and the locations of the neutral surface elements in the rotational coordinates can be defined by introducing curvilinear surface coordinates α_1, α_2, and α_3. In Fig. 1, r represents the mean radius of the ring and u_r and u_θ represent, respectively, the transverse and circumferential displacements. This form of arrangement is typical in the design of an angular rate sensor that uses a ring-type structural element.

Considering that the ring rotates about the z-axis with an angular rate, $\Omega(t)$, and neglecting the rotary inertia effects, the kinetic energy of the rotating ring can be expressed by

$$T = \frac{\rho A r}{2}\int_0^{2\pi} |\mathbf{v}|^2 \,\mathrm{d}\theta, \tag{1}$$

where ρ represents the material density of the ring and A represents the cross-sectional area of the ring. The amplitude square of the velocity, $|\mathbf{v}|^2$, for the ring element in the $X-Y-Z$ frame can be written by

$$|\mathbf{v}|^2 = (\dot{u}_r^2 + \dot{u}_\theta^2) + \Omega^2(u_\theta^2 + u_r^2 + 2ru_r + r^2) + 2\Omega(\dot{u}_\theta u_r - \dot{u}_r u_\theta + r\dot{u}_\theta). \tag{2}$$

In order to obtain an expression for the strain energy, a relationship between the strain and the displacement can be written as follows [10]:

$$\varepsilon_r = 0, \quad \varepsilon_\theta = \varepsilon_\theta^o + \alpha_3 K_\theta, \tag{3}$$

$$\varepsilon_\theta^o = \frac{1}{r}\left(\frac{\partial u_\theta}{\partial\theta} + u_r\right), \quad K_\theta = \frac{1}{r}\frac{\partial\beta}{\partial\theta} = \frac{1}{r^2}\left(\frac{\partial u_\theta}{\partial\theta} - \frac{\partial^2 u_r}{\partial\theta^2}\right), \tag{4}$$

where ε_r and ε_θ, respectively, represent the radial and tangential strain components. The change of curvature is denoted by K_θ and is related to the rotation angle β. The membrane strain is denoted by ε_θ^o while the relative location from the neutral surface is represented by α_3. In addition, the strain caused by the centrifugal forces that result from the ring rotation must be considered and can be expressed in the following form [4]:

$$\varepsilon_\theta^i = \frac{1}{2r^2}\left[\left(u_r + \frac{\partial u_\theta}{\partial\theta}\right)^2 + \left(\frac{\partial u_r}{\partial\theta} - u_\theta\right)^2\right]. \tag{5}$$

The strain energy of the ring can now be formulated using the expressions for the strains given in Eqs. (3) and (5):

$$U = br\int_{-h/2}^{h/2}\int_0^{2\pi}\left[\tfrac{1}{2}\sigma_\theta(\varepsilon_\theta + \varepsilon_\theta^i) + \sigma_\theta^i(\varepsilon_\theta + \varepsilon_\theta^i)\right]\mathrm{d}\theta\,\mathrm{d}\alpha_3, \tag{6}$$

where h denotes the radial thickness while b denotes the axial thickness of the ring as illustrated in Fig. 1. The normal stress component in the circumferential direction is denoted by σ_θ while the normal stress caused by the centrifugal force is denoted by σ_θ^i which is approximately equal to $\rho r^2\Omega^2$ [11].

The equations that govern the in-plane motion of the ring can be derived via the Hamilton's principle [10]

$$\delta\int_{t_0}^{t_1}(U - T)\,\mathrm{d}t = 0, \tag{7}$$

where δ represents the variational symbol and time variables t_0 and t_1 are arbitrary. The equations of motion are

$$-\frac{EA}{br^2}(u_\theta'' + u_r') - \frac{EI}{br^4}(u_\theta'' - u_r''') + \rho h\Omega^2(-2u_r' - u_\theta'') + k_\theta u_\theta + \rho h\left(\ddot{u}_\theta + \dot{\Omega}u_r + 2\Omega\dot{u}_r\right) = 0, \tag{8}$$

$$\frac{EA}{br^2}(u_\theta' + u_r) - \frac{EI}{br^4}(u_\theta''' - u_r'''') + \rho h\Omega^2\left(2u_\theta' - u_r''\right) + k_r u_r + \rho h\left(\ddot{u}_r - \dot{\Omega}u_\theta - 2\Omega\dot{u}_\theta\right) = 0, \tag{9}$$

where E represents the Young's modulus, and the area moment of inertia of the ring cross section about its neutral axis is expressed as $I = bh^3/12$. In Eqs. (8) and (9) the time derivatives are indicated by $\dot{(\,)}$, while the spatial derivatives are indicated by $(\,)'$. It is worth noting that the rotational rate Ω is assumed to be time-dependent in this study, and as a result the equations of motion include terms that contain the angular

acceleration term $\dot{\Omega}$. Due to the periodic nature of solutions, the circumferential (extensional) and radial displacement can be assumed as follows:

$$u_r(\theta, t) = \sum_{n=0}^{\infty} \left[q_1(t) \cos(n\theta) + q_2(t) \sin(n\theta) \right], \tag{10}$$

$$u_\theta(\theta, t) = \sum_{n=0}^{\infty} \left[q_3(t) \cos(n\theta) + q_4(t) \sin(n\theta) \right], \tag{11}$$

where the generalized coordinates, q_1 and q_2, represent flexural modes of the in-plane ring vibration while the coordinates, q_3 and q_4, represent extensional modes of the in-plane ring vibration. It may be noted that in vibratory angular rate sensor applications, only one of the second flexural modes is excited since it provides the largest angular-shift due to external rate input [3]. Thus, the second flexural modes are chosen for investigating natural frequency variation with the input angular rate and for performing stability analysis via suitable modelling. The second in-plane flexural mode shapes and the associated generalized coordinates of a ring are shown in Fig. 2. The two degenerate modal configurations are separated by 45° due to ring symmetry as depicted in the figure. Also, reversal of the nodes and the anti-nodes associated with the two configurations are illustrated in this figure. Utilizing an approximate relationship between the extensional and the flexural modes [4], the four generalized coordinates can be reduced to two generalized coordinates that are associated with the flexural modes of the in-plane ring vibration:

$$q_3 = -(1/n)q_1, \quad q_4 = (1/n)q_2, \tag{12}$$

where n represents the mode number which in the present case is equal to a value 2 and the discretized equation of motion in the flexural coordinate vector $\mathbf{q} = \left[q_1\, q_2\right]^{\mathrm{T}}$ is derived by

$$\mathbf{M}\ddot{\mathbf{q}} + (\mathbf{G} + \mathbf{D})\dot{\mathbf{q}} + \mathbf{K}\mathbf{q} = \mathbf{0}. \tag{13}$$

In Eq. (13), the system matrices can be expressed by

$$\mathbf{M} = \begin{bmatrix} 1 & 0 \\ 0 & 1 + \delta m \end{bmatrix}, \quad \mathbf{G} = \begin{bmatrix} 0 & -2\Omega\gamma \\ 2\Omega\gamma & 0 \end{bmatrix},$$

$$\mathbf{D} = \begin{bmatrix} 2\zeta\omega_{o1} & 0 \\ 0 & 2\zeta\omega_{o2} \end{bmatrix}, \quad \mathbf{K} = \begin{bmatrix} \kappa_1 + \kappa_2\Omega^2 & -\dot{\Omega}\gamma \\ \dot{\Omega}\gamma & \kappa_1 + \kappa_2\Omega^2 \end{bmatrix}, \tag{14}$$

with

$$\gamma = \frac{(\tilde{b} + n^2\tilde{a})}{n(\tilde{a} + \tilde{b})}, \quad \kappa_1 = \frac{\tilde{b}\tilde{c} - n^2\tilde{a}^2}{\rho A(\tilde{a} + \tilde{b})}, \quad \kappa_2 = \frac{n^2(\tilde{b} + \tilde{c} - 4\tilde{a})}{\tilde{a} + \tilde{b}} - \frac{(2 + n^2)(\tilde{b}\tilde{c} - n^2\tilde{a})}{(\tilde{a} + \tilde{b})^2},$$

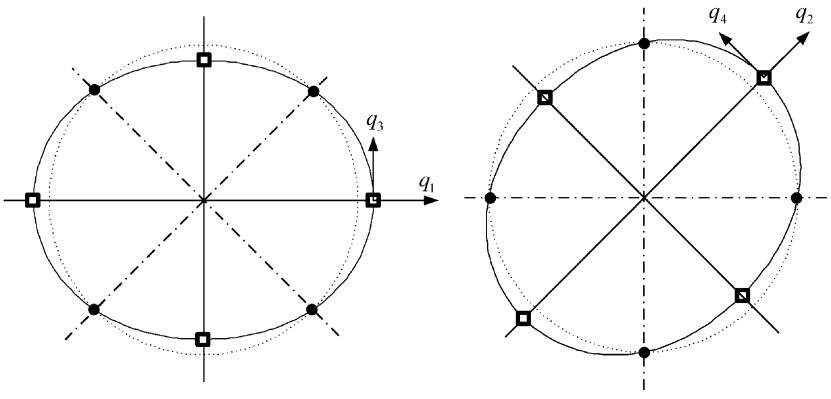

Fig. 2. Second flexural mode shapes of a ring: ●, node; ■, anti-node; ·–·–, nodal line.

$$\tilde{a} = n^2\frac{EI}{r^4} + \frac{EA}{r^2}, \quad \tilde{b} = n^2\left(\frac{EI}{r^4} + \frac{EA}{r^2}\right), \quad \tilde{c} = n^4\frac{EI}{r^4} + \frac{EA}{r^2}, \qquad n = 2,$$

where **M** is the mass matrix in which a mass mismatch δm is added to represent the ring asymmetry, **G** is the skew-symmetric gyroscopic matrix which results from Coriolis acceleration, **D** is the damping matrix, and **K** is the stiffness matrix. The matrices **M**, **D**, and **K** are symmetric. The approximated parameters γ, κ_1, and κ_2 are constant values that depend on the mode number n and the physical properties of a ring. In the Damping matrix, ζ represents the damping ratio, and ω_{o1} and ω_{o2}, respectively, represent non-rotating ring fundamental natural frequencies that are associated with the flexural generalized coordinates q_1 and q_2. Further details of derivation of the equations can be found in the paper by Huang and Soedel [4].

3. Stability analysis

For the purpose of investigating the stability of a rotating ring subjected to periodic perturbation in the angular rate, the input angular rate is assumed to take the form:

$$\Omega(t) = \bar{\Omega}(1 + \mu\cos\nu t), \quad 0 < \mu \ll 1, \tag{15}$$

where $\bar{\Omega}$ is the amplitude of the input angular rate, μ represents the small dimensionless amplitude of fluctuation, and ν represents the frequency of the imposed periodic excitation. For the purpose of investigating the stability behaviour in a small neighbourhood around certain critical frequency ω_o, the excitation frequency is written in the form

$$\nu = \omega_0(1 - \lambda), \quad |\lambda| \leqslant 1, \tag{16}$$

where λ denotes a detuning parameter. When the system is under the specified periodic excitation, the motion of the rotating ring can be represented by a parametrically excited gyroscopic system. It is known that closed form solutions for this class of systems are not available. However, asymptotic methods such as the method of multiple scales [12], and the method of averaging [13] can be employed to construct asymptotic solutions. The method of averaging has been successfully employed for studying stability of rotating mechanical systems that are of a similar class [7]. Before performing any analytical stability analysis, it is first necessary to decouple the equations of motion, which are coupled via the gyroscopic and stiffness terms. It is known that the skew-symmetric gyroscopic coupling in the equations cannot be removed using the classical point transformation. A contact transformation [7] is used in the present paper to decouple the system, and for this purpose, the equations are formulated in the Hamiltonian form.

To this end, Eq. (13) is rearranged to the following form:

$$\mathbf{M}\ddot{\mathbf{q}} + \mathbf{G}_c\dot{\mathbf{q}} + \mathbf{K}_c\mathbf{q} = \mathbf{F}(\mathbf{q}, \dot{\mathbf{q}}, t) \tag{17}$$

with

$$\mathbf{F} = -\mathbf{D}\dot{\mathbf{q}} - f_c(t)(\hat{\mathbf{G}}_c\dot{\mathbf{q}} + \hat{\mathbf{K}}_c\mathbf{q}) - \nu f_s(t)\hat{\mathbf{K}}_s\mathbf{q}, \quad f_c(t) = \cos\nu t, \quad f_s(t) = \sin\nu t,$$

where $\mathbf{G}_c$, $\hat{\mathbf{G}}_c$, $\mathbf{K}_c$, $\hat{\mathbf{K}}_c$, and $\hat{\mathbf{K}}_s$ contain the time-invariant portion of **G** and **K** matrices, and the right-hand side of Eq. (17) contains smaller amplitude excitation and the damping terms which are considered small. Now, by letting the right-hand side to be zero, the homogeneous equation can be obtained by

$$\mathbf{M}\ddot{\mathbf{q}} + \mathbf{G}_c\dot{\mathbf{q}} + \mathbf{K}_c\mathbf{q} = \mathbf{0}. \tag{18}$$

Since the mass matrix **M** is positive definite, the corresponding Hamiltonian function **H** can be formulated using the generalized coordinate vector **q** and by introducing the momentum conjugate vector **P**. A set of first-order Hamilton's equations that are equivalent to the original second-order form can be obtained in terms of the variable $\check{\mathbf{u}}$ where $\check{\mathbf{u}} = [\mathbf{q} \quad \mathbf{p}]^{\mathrm{T}}$ [7]. A contact transformation of the form $\check{\mathbf{u}} = \mathbf{T}\cdot\check{\mathbf{v}}$ can then be employed to decouple the system of equations that are now expressed in terms of the transformed variable $\check{\mathbf{v}}$ that contains the transformed generalized coordinate vector, **Q**, and the momentum conjugate vector, **P**. The transformed equations are

$$\check{\mathbf{v}}' = \mathbf{J}\hat{\mathbf{H}}^o\check{\mathbf{v}} + [\lambda\mathbf{J}\hat{\mathbf{H}}^o - \mathbf{D}^o - \mathbf{A}^o\cos\tau - \mathbf{B}\sin\tau]\check{\mathbf{v}}, \quad \check{\mathbf{v}} = [\mathbf{Q} \quad \mathbf{P}]^{\mathrm{T}}, \tag{19}$$

where the non-dimensional time, $\tau = vt$, is introduced for simplicity, and the prime denotes differentiation with respect to non-dimensional time τ. The system matrices associated with Eq. (19) are derived to be

$$\hat{\mathbf{H}}^o = \text{diag}\{K_1, K_2; K_1, K_2\} \quad \text{and} \quad K_i = \omega_i/\omega_0 \quad (i = 1, 2),$$

$$\mathbf{D}^o = (\mathbf{T}^{-1}\,\tilde{\mathbf{D}}\,\mathbf{JHT})/\omega_0, \quad \mathbf{A}^o = (\mathbf{T}^{-1}\hat{\tilde{\mathbf{G}}}_c\mathbf{JHT} + \mathbf{T}^{-1}\hat{\tilde{\mathbf{K}}}_c\mathbf{T})/\omega_0, \quad \mathbf{B} = \mathbf{T}^{-1}\hat{\tilde{\mathbf{K}}}_s\mathbf{T},$$

$$\mathbf{J} = \begin{bmatrix} \mathbf{0} & \mathbf{I} \\ -\mathbf{I} & \mathbf{0} \end{bmatrix}, \quad \tilde{\mathbf{D}} = \begin{bmatrix} \mathbf{0} & \mathbf{0} \\ \mathbf{D} & \mathbf{0} \end{bmatrix}, \quad \hat{\tilde{\mathbf{G}}}_c = \begin{bmatrix} \mathbf{0} & \mathbf{0} \\ \hat{\mathbf{G}}_c & \mathbf{0} \end{bmatrix}, \quad \hat{\tilde{\mathbf{K}}}_c = \begin{bmatrix} \mathbf{0} & \mathbf{0} \\ \hat{\mathbf{K}}_c & \mathbf{0} \end{bmatrix}, \quad \hat{\tilde{\mathbf{K}}}_s = \begin{bmatrix} \mathbf{0} & \mathbf{0} \\ \hat{\mathbf{K}}_s & \mathbf{0} \end{bmatrix},$$

where the terms ω_i $(i = 1,2)$ represent the rotating ring natural frequencies that are associated with the flexural generalized coordinates q_1 and q_2. Martices $\mathbf{I}$ and $\mathbf{0}$ represent, respectively, 2×2 identity matrix and null matrix, while $\mathbf{T}$ denotes the transformation matrix. The details of the elements of matrices $\mathbf{T}$, $\mathbf{D}^o$, $\mathbf{A}^o$, and $\mathbf{B}$ are given in Appendix A.

Since the method of averaging requires the system equations to be expressed in terms of the amplitude and phase variables, generalized coordinates $\mathbf{Q}$ and momentum vector $\mathbf{P}$ in Eq. (19) are transformed to amplitude and phase variables $a(\tau)$ and $\phi(\tau)$ via:

$$Q_i = a_i(\tau)\,\sin\,\Phi_i(\tau), \quad P_i = a_i(\tau)\,\cos\,\Phi_i(\tau), \quad \Phi_i(\tau) = K_i\tau + \phi_i(\tau), \qquad i = 1, 2. \tag{20a,b}$$

After this transformation procedure, the equations in the so called "standard form" can be expressed by

$$a_i' = g_i\,\sin\,\Phi_i + g_{(i+2)}\,\cos\,\Phi_i, \tag{21a}$$

$$a_i\phi_i' = \lambda K_i a_i + g_i\,\cos\,\Phi_i - g_{(i+2)}\,\sin\,\Phi_i, \quad i = 1, 2, \tag{21b}$$

where

$$g_k = \sum_{l=1}^{2}\Big\{-[D_{kl}^o a_l\,\sin\,\Phi_l + D_{k(l+2)}^o a_l\,\sin\,\Phi_l] - \cos\,\tau[A_{kl}^o a_l\,\sin\,\Phi_l + A_{k(l+2)}^o a_l\,\sin\,\Phi_l]$$
$$- \sin\,\tau[B_{kl}a_l\,\sin\,\Phi_l + B_{k(l+2)}a_l\,\sin\,\Phi_l]\Big\}, \quad k = i, i+2. \tag{22}$$

Since Eqs. (21) are exactly equivalent to Eq. (17), by applying an averaging operator

$$M(\cdot) = \lim_{T\to\infty}\frac{1}{T}\int_{\tau}^{\tau+T}(\cdot)\,\mathrm{d}\tau, \tag{23}$$

the averaged amplitude and phase valuables can be obtained, where it is understood that the integration is performed over explicit time τ for one period T [13]. Examination of the averaged equations indicate that the stability of the solutions depends on whether or not the excitation frequency v is in the neighbourhood of certain critical frequencies. Omitting the higher-order resonances that are not of significance [14], in the present study the method averaging was performed for three different cases.

3.1. Case I—non-resonance

The stability of solutions is examined for the conditions of $K_i \neq (1/2)$ and $|K_i \pm K_j| \neq 1$ $(i,j = 1,2)$ $i \neq j$. Applying the averaging operator M to Eqs. (21), a set of averaged equations can be obtained as follows:

$$\bar{a}_i' = -\frac{\bar{a}_i}{2}\left(D_{ii}^o + D_{(i+2)(i+2)}^o\right), \quad \bar{\phi}'_i = \lambda K_i - \frac{1}{2}\left(D_{i(i+2)}^o - D_{(i+2)i}^o\right), \qquad i = 1, 2, \tag{24a,b}$$

Now inserting Eqs. (26) into Eq. (22), and then solving for $\mathbf{Q}$ and $\mathbf{P}$ results in

$$Q_i = \bar{a}_{iC}\,\mathrm{e}^{-\frac{1}{2}\left(D_{ii}^o + D_{(i+2)(i+2)}^o\right)\tau}\,\sin\left[\omega_i t - \frac{1}{2}\left(D_{i(i+2)}^o - D_{(i+2)i}^o\right)\tau + \bar{\phi}_{iC}\right], \tag{25a}$$

$$P_i = \bar{a}_{iC} e^{-\frac{1}{2}\left(D^o_{ii}+D^o_{(i+2)(i+2)}\right)\tau} \cos\left[\omega_i t - \frac{1}{2}\left(D^o_{i(i+2)} - D^o_{(i+2)i}\right)\tau + \bar{\phi}_{iC}\right], \quad i = 1,2, \tag{25b}$$

where $\bar{a}_{iC}$ and $\bar{\phi}_{iC}$ are arbitrary constants. When the non-dimensional time τ approaches infinity, the variables Q_i and P_i approach zero meaning that the system is stable. Hence, in the non-resonance case, the periodic parametric excitation cannot lead the system into instability.

3.2. Case II—sub-harmonic resonance

Under the sub-harmonic resonance conditions, $K_i = 1/2$ ($\omega_0 = 2\omega_i$, $i = 1,2$), the stability of the solution is examined by employing the averaged equations:

$$\bar{a}_i' = \bar{a}_i\left(Z_i + \tfrac{1}{2}U_i \sin 2\bar{\phi}_i + \tfrac{1}{2}V_i \cos 2\bar{\phi}_i\right), \tag{26a}$$

$$\bar{\phi}'_i = \left\{\lambda K_i + \left[-\tfrac{1}{2}V_i \sin 2\bar{\phi}_i - (-1)^i \tfrac{1}{2}U_i \cos 2\bar{\phi}_i\right]\right\}, \quad i = 1,2 \tag{26b}$$

where

$$Z_i = -\frac{1}{2}\left(D^o_{ii} + D^o_{(i+2)(i+2)}\right), \quad U_i = -\frac{1}{2}\left(A^o_{i(i+2)} + A^o_{(i+2)i} + B_{ii} - B_{(i+2)(i+2)}\right),$$

$$V_i = -\frac{1}{2}\left(-A^o_{ii} + A^o_{(i+2)(i+2)} + B_{i(i+2)} + B_{(i+2)i}\right), \quad i = 1,2.$$

In order to investigate the stability of solutions of Eqs. (21), new variables, x_i and y_i, are introduced via:

$$x_i = \bar{a}_i \cos\bar{\phi}_i, \quad y_i = \bar{a}_i \sin\bar{\phi}_i, \qquad i = 1,2.$$

Solutions of the form $e^{\rho\tau}$ are now sought which yields the characteristic equation for the exponent ρ as

$$\rho^2 - 2Z_i\rho + \frac{1}{4}\left(\lambda^2 - V_i^2 - U_i^2 + 4Z_i^2\right) = 0, \quad i = 1,2. \tag{27}$$

The system will be unstable when $\rho_{1,2} > 0$, and hence from Eq. (27), closed form instability conditions can be derived by

$$1 - \sqrt{V_i^2 + U_i^2 - 4Z_i^2} < \frac{\nu}{\omega_0} < 1 + \sqrt{V_i^2 + U_i^2 - 4Z_i^2}, \quad \omega_0 = 2\omega_i, \ i = 1,2. \tag{28}$$

3.3. Case III—combination resonance

Applying the average operator for the sum-type combination resonance case, $|K_2 + K_1| = 1$, ($\omega_0 = \omega_2 + \omega_1$), the system Eqs. (21) are averaged to a set of four coupled first-order differential equations in the amplitudes and phase:

$$\bar{a}_1' = \left[Z_1\bar{a}_1 + \tfrac{1}{2}\bar{a}_2 U_3 \sin(\bar{\phi}_2 + \bar{\phi}_1) + \tfrac{1}{2}\bar{a}_2 V_3 \cos(\bar{\phi}_2 + \bar{\phi}_1)\right], \tag{29a}$$

$$\bar{a}_2' = \left[Z_2\bar{a}_2 + \tfrac{1}{2}\bar{a}_1 U_4 \sin(\bar{\phi}_2 + \bar{\phi}_1) + \tfrac{1}{2}\bar{a}_1 V_4 \cos(\bar{\phi}_2 + \bar{\phi}_1)\right], \tag{29b}$$

$$\bar{a}_1\bar{\phi}_1' = \lambda K_1\bar{a}_1 + \left[-\tfrac{1}{2}\bar{a}_2 V_3 \sin(\bar{\phi}_2 + \bar{\phi}_1) + \tfrac{1}{2}\bar{a}_2 U_3 \cos(\bar{\phi}_2 + \bar{\phi}_1)\right], \tag{29c}$$

$$\bar{a}_2\bar{\phi}_2' = \lambda K_2\bar{a}_2 + \left[-\tfrac{1}{2}\bar{a}_1 V_4 \sin(\bar{\phi}_2 + \bar{\phi}_1) + \tfrac{1}{2}\bar{a}_1 U_4 \cos(\bar{\phi}_2 + \bar{\phi}_1)\right], \tag{29d}$$

where

$$U_3 = -\tfrac{1}{2}(A^o_{14} + A^o_{32} + B_{12} - B_{34}), \quad U_4 = -\tfrac{1}{2}(A^o_{23} + A^o_{41} + B_{21} - B_{43}),$$

$$V_3 = -\tfrac{1}{2}(-A^o_{12} + A^o_{34} + B_{14} + B_{32}), \quad V_4 = -\tfrac{1}{2}(-A^o_{21} + A^o_{43} + B_{23} + B_{41}).$$

Employing a transformation in the complex plane, Eqs. (29), can be decoupled [14], and then by seeking the solutions of the form $e^{\rho\tau}$, the characteristic equation is obtained. In the absence of damping this equation takes the form

$$(\rho - j\lambda K_1)(\rho + j\lambda K_2) - \left(\frac{1}{2}\right)^2 (V_3 + jU_3)(V_4 - jU_4) = 0. \tag{30}$$

By setting $\rho_{1,2} > 0$ for system instability, the closed form instability conditions are obtained as follows for the undamped case:

$$1 - \sqrt{(V_3V_4 + U_3U_4) - j(U_3V_4 - V_3U_4)} < \frac{v}{\omega_0} < 1 + \sqrt{(V_3V_4 + U_3U_4) - j(U_3V_4 - V_3U_4)}. \tag{31}$$

Now, if damping is introduced in the system, the characteristic equation becomes

$$\rho^2 - (Z_1 + Z_2 - j\lambda K_2 + j\lambda K_1)\rho + (Z_1 + j\lambda K_1)(Z_2 - j\lambda K_2) - \left(\frac{1}{2}\right)^2 (U_3U_4) = 0. \tag{32}$$

Then, the instability condition for the damped case can be expressed by

$$1 - \sqrt{U_3U_4 \frac{(Z_1 + Z_2)^2}{4Z_1Z_2} - (Z_1 + Z_2)^2} < \frac{v}{\omega_0} < 1 + \sqrt{U_3U_4 \frac{(Z_1 + Z_2)^2}{4Z_1Z_2} - (Z_1 + Z_2)^2}. \tag{33}$$

Similarly, for the case of difference-type combination resonance, $|K_2 - K_1| = 1 (\omega_0 = \omega_2 - \omega_1)$, by applying the same procedure, the instability conditions for the undamped case,

$$1 - \sqrt{(V_3^oV_4^o + U_3^oU_4^o) - j(U_3^oV_4^o - V_3^oU_4^o)} < \frac{v}{\omega_0} < 1 + \sqrt{(V_3^oV_4^o + U_3^oU_4^o) - j(U_3^oV_4^o - V_3^oU_4^o)} \tag{34}$$

and for the damped case,

$$1 - \sqrt{U_3^oU_4^o \frac{(Z_1 + Z_2)^2}{4Z_1Z_2} - (Z_1 + Z_2)^2} < \frac{v}{\omega_0} < 1 + \sqrt{U_3^oU_4^o \frac{(Z_1 + Z_2)^2}{4Z_1Z_2} - (Z_1 + Z_2)^2} \tag{35}$$

are obtained, where

$$U_3^o = -\frac{1}{2}(-A_{14}^o + A_{32}^o - B_{12} - B_{34}), \quad U_4^o = -\frac{1}{2}(A_{23}^o - A_{41}^o - B_{21} - B_{43}),$$
$$V_3^o = -\frac{1}{2}(A_{12}^o + A_{34}^o - B_{14} + B_{32}), \quad V_4^o = -\frac{1}{2}(A_{21}^o + A_{43}^o + B_{23} - B_{41}). \tag{36}$$

For a set of system parameters, the conditions given by Eqs. (28), (31), (33), (34) and (35) are computed so that the onset of angular rate sensor instabilities can be characterized.

4. Results and discussion

In order to illustrate the applicability of the analytical results, typical parameters associated with a ring-type angular sensor are considered. The parameters of a micromachined ring used are shown in Table 1. In the present study, it is assumed that the ring is fabricated of nickel which has isotropic material properties.

Table 1
Ring parameters for numerical calculations

Density (Nickel)	$\rho = 8800\,\mathrm{kg/m^3}$
Young's modulus (Nickel)	$E = 210 \times 10^9\,\mathrm{N/m^2}$
Mean radius	$r = 500\,\mu\mathrm{m}$
Radial thickness	$h = 12.5\,\mu\mathrm{m}$
Axial thickness	$b = 30\,\mu\mathrm{m}$

Owing to the speed-dependent gyroscopic coupling and system stiffness, it is known that bifurcations of natural frequencies can take place. In order to illustrate this effect, the second flexural mode is considered and the variations of the corresponding natural frequencies with input angular rate are depicted in Fig. 3. As a result of an assumed mass mismatch, δm, of 0.01%, it can be observed that the natural frequencies associated with a non-rotating ring system (i.e., input angular rate is zero) are not identical: $\omega_{01} = 1.8918 \times 10^5$ (rad/s) and $\omega_{02} = 1.8919 \times 10^5$ (rad/s). It may be noted that this natural frequency variation with the input angular rate as described above is essential for stability investigation since the instability regions are investigated near certain combinations and multiple of these system natural frequencies.

Assuming a presence of a small mass mismatch ($\delta m \neq 0$), and absence of damping ($\zeta = 0$) in the system, the instability conditions obtained from Eqs. (28), (31) and (34) are plotted in the excitation frequency-amplitude space ($\nu - \mu$) in Fig. 4. It may be noted that μ represents the small dimensionless amplitude of fluctuation, and ν represents the frequency of the imposed periodic excitation. The hatched parts represent the unstable regions and the clear parts illustrate the stable regions. It can be seen that the instability region associated with the sum-type combination resonance, $|K_2 + K_1| = 1$ ($\omega_0 = \omega_2 + \omega_1$), obtained from Eqs. (31) is relatively larger than the regions associated with the sub-harmonic resonances, $K_i = 1/2$ ($\omega_0 = 2\omega_i$, $i = 1, 2$), obtained from Eq. (28). Also, it may be noted that with the presence of some mass mismatch in the system, employing Eq. (34) no instability region is found to exist for the difference-type combination resonance, $|K_2 - K_1| = 1(\omega_0 = \omega_2 - \omega_1)$. When the ring is assumed to be perfect, i.e., $\delta m = 0$, instability regions do not exist as mentioned in the study of Kammer and Schlack [6].

The plots in Fig. 5 illustrate the variations of the instability regions when damping is considered. As damping increases, the instability regions shift upwards in both the sub-harmonic and combination resonance cases, which results in a more stable system. However, the damped instability region in the case of sub-harmonic resonance appears narrower than the region associated with the corresponding undamped system as shown in Fig. 5(a), while in the case of the combination resonance, the damped instability region is wider as the region shifts upward as depicted in Fig. 5(b). Further, for the undamped system the instability regions for the sum-type combination resonance case can be obtained using Eq. (31), which is derived for the case of $\zeta = 0$ and from Eq. (33) when the damping ratio approaches zero, i.e., $\lim_{\zeta \to 0} Z_i (i = 1, 2)$. As shown in Fig. 5(b), these two regions differ and the difference is illustrated by introducing a quasi-stabile region for the latter case.

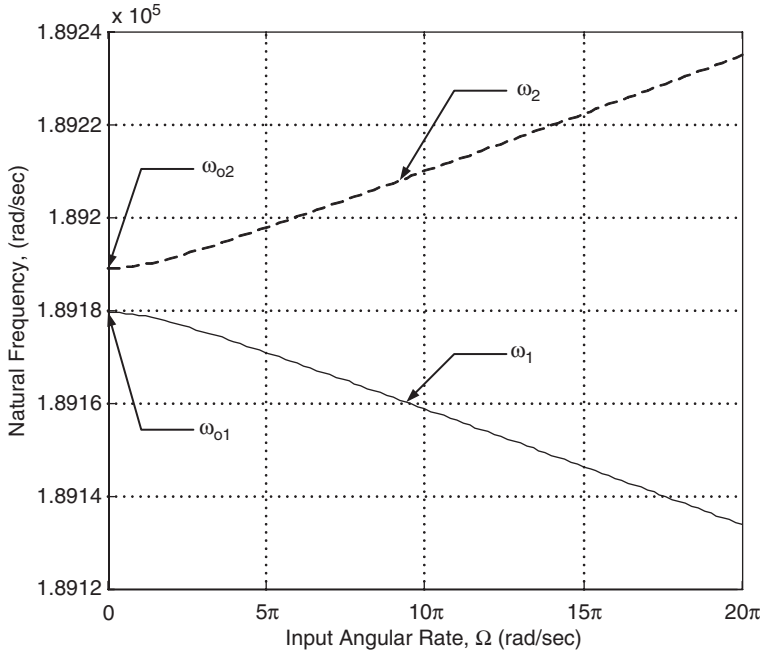

Fig. 3. Natural frequency variations for a rotating ring with non-zero mass mismatch ($\delta m \neq 0$).

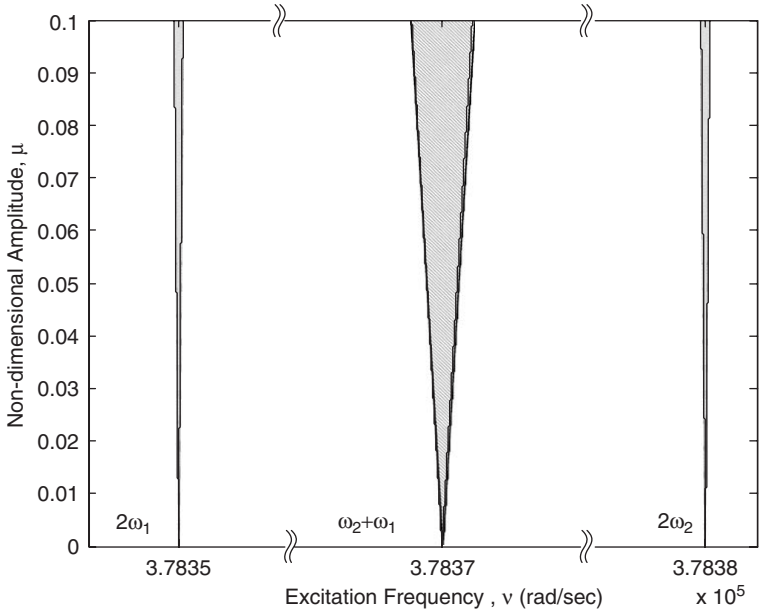

Fig. 4. Instability regions: undamped ($\zeta = 0$) with non-zero mass mismatch ($\delta m \neq 0$): ▨, unstable regions.

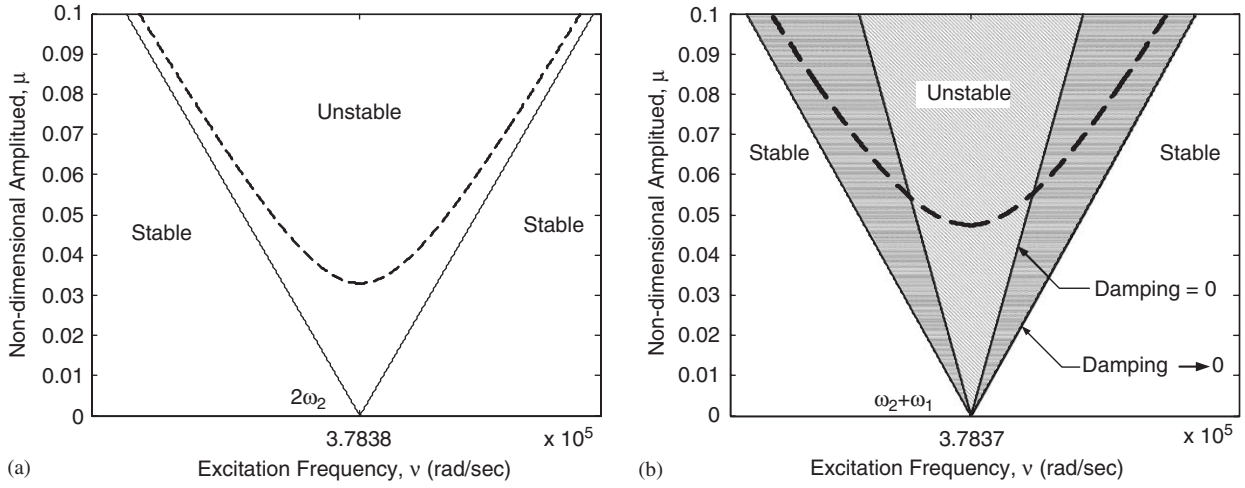

Fig. 5. Instability regions for damped and undamped cases: (a) subharmonic resonance: —, undamped; – – –, damped and (b) combination resonance: —, undamped; – – –, damped; ▨, unstable region; ▨, quasi-stable region.

It may be noted that this phenomenon is only observable for the combination resonance case. Generally, the damping in the micromachined gyros is generated from air and heat: air-damping and thermoelastic damping affect the resonant frequency and quality factor. Although it is known that elimination of damping increases the quality factor of the gyro, the presence of damping provides larger stable region thus stabilizing the gyroscopic system.

In order to examine the effects the input angular rate and the mass mismatch have on the stability, the variation of the associated regions with respect to the above two parameters are plotted. Figs. 6(a) and (b) clearly illustrate that widening of regions take place with increasing angular rates and increasing mass mismatch.

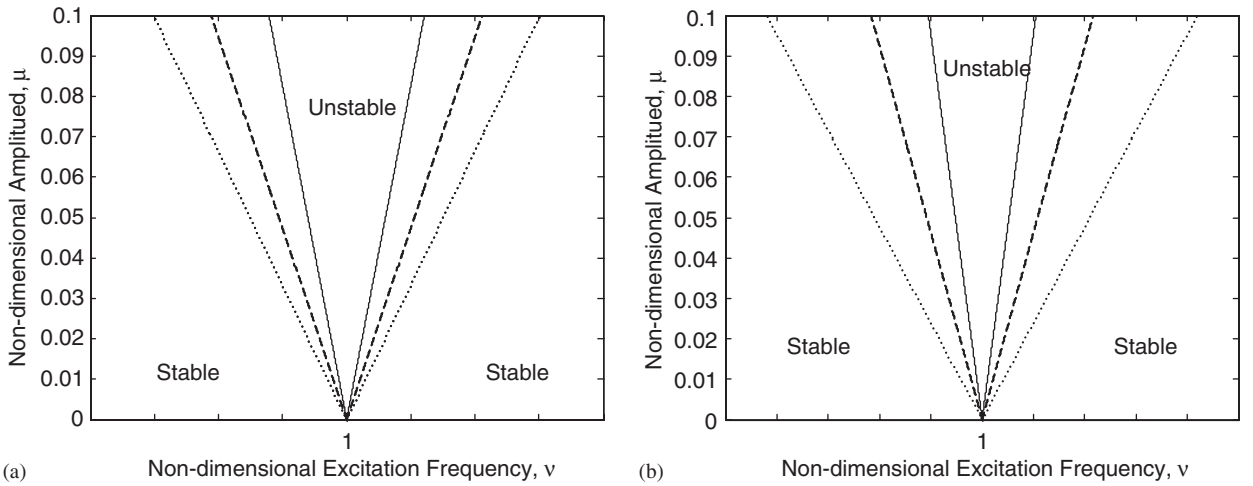

Fig. 6. Insability regions: (a) variation with input angular rate, $\bar{\Omega}$ (rad/s): —, 2π; – – –, 3π; · · · · ·, 4π and (b) variation with mass mismatch, δm (%): —, 0.01; – – –, 0.025; · · · · ·, 0.05.

For the choice of parameters considered in this paper, the instability behaviour predicted from the present analysis clearly demonstrate the use of this analysis in the design of this class of devices. It may be noted that the material used in this study is nickel since it is the most common choice until now. However, recent efforts are going into producing structures using polysilicon which is known to have a certain degree of anisotropy. Hence, future stability analyses will need to incorporate this property if accurate instability predictions are warranted.

5. Conclusions

Dynamic stability analysis for a micromachined ring-type structure subjected to base rotation with periodic perturbations is performed. The angular motion of the ring affects not only the gyroscopic coupling but also the variation of the stiffness. Method of averaging has been employed for deriving the instability conditions in closed-form. These conditions predict the onset of instability behaviour characterized by exponential growth in response amplitudes, and are illustrated by plotting the instability regions in the excitation frequency-excitation amplitude space. If the mass mismatch in the ring is considered, instability regions are observed when the excitation frequencies are near the sub-harmonic or sum-type combination resonance frequencies. In the case of no mass mismatch, instability regions do not exist. Instability regions associated with the damped systems are found to be narrower in the case of sub-harmonic resonance and wider in the case of the combination resonance. In addition, in all cases considered, the instability regions are observed to become wider with increasing input angular rates and mass mismatch. The understanding of the instability behaviour as predicted in the present study is expected to result in a better insight into the dynamic behaviour associated with angular rate sensors that are of the rotating ring-type.

Acknowledgements

This research was supported in part by the Natural Science and Engineering Research Council (NSERC) of Canada discovery grant and the Special University Scholarships (SUS) scheme from The University of Western Ontario, London, Ontario, Canada.

Appendix A. System matrices

The system matrices are evaluated to be

$$\mathbf{D}^o = \frac{1}{\omega_0}\begin{bmatrix} D_{11} & D_{12} & 0 & 0 \\ D_{21} & D_{22} & 0 & 0 \\ 0 & 0 & D_{33} & D_{34} \\ 0 & 0 & D_{43} & D_{44} \end{bmatrix}, \quad \mathbf{A}^o = \frac{1}{\omega_0}\begin{bmatrix} 0 & 0 & A_{13} & A_{14} \\ 0 & 0 & A_{23} & A_{24} \\ A_{31} & A_{32} & 0 & 0 \\ A_{41} & A_{42} & 0 & 0 \end{bmatrix},$$

$$\mathbf{B} = \begin{bmatrix} B_{11} & B_{12} & 0 & 0 \\ B_{21} & B_{22} & 0 & 0 \\ 0 & 0 & B_{33} & B_{34} \\ 0 & 0 & B_{43} & B_{44} \end{bmatrix}, \quad \mathbf{T} = \begin{bmatrix} \frac{X_{11}}{N_1} & \frac{X_{21}}{N_2} & 0 & 0 \\ 0 & 0 & \frac{Y_{11}}{N_1} & \frac{Y_{21}}{N_2} \\ 0 & 0 & \frac{Y_{12}}{N_1} & \frac{Y_{22}}{N_2} \\ \frac{X_{12}}{N_1} & \frac{X_{22}}{N_2} & 0 & 0 \end{bmatrix},$$

$$N_i = \sqrt{x_i^{\mathrm{T}} J y_i} = \sqrt{X_{i1}Y_{i2} - X_{i2}Y_{i1}} \quad (i = 1, 2),$$

where $\mathbf{x}_i = \begin{bmatrix} X_{i1} & 0 & 0 & X_{i2} \end{bmatrix}^{\mathrm{T}}$ and $\mathbf{y}_i = \begin{bmatrix} 0 & Y_{i1} & Y_{i2} & 0 \end{bmatrix}^{\mathrm{T}}$ represent, respectively, real and imaginary parts of the eigenmodes of Eq. (18). The other components of the matrices can be written by

$$D_{11} = \frac{2\zeta\omega_{02}(\gamma\bar{\Omega}X_{11}X_{21} - X_{12}X_{21})}{(1+\delta m)\Lambda}, \quad D_{12} = \frac{2\zeta\omega_{02}(\gamma\bar{\Omega}X_{21}^2 - X_{21}X_{22})}{(1+\delta m)\Lambda}\frac{N_1}{N_2},$$

$$D_{21} = -\frac{2\zeta\omega_{02}(\gamma\bar{\Omega}X_{11}^2 - X_{11}X_{12})}{(1+\delta m)\Lambda}\frac{N_2}{N_1}, \quad D_{22} = -\frac{2\zeta\omega_{02}(\gamma\bar{\Omega}X_{11}X_{21} - X_{11}X_{22})}{(1+\delta m)\Lambda},$$

$$D_{33} = -\frac{2\zeta\omega_{01}(\gamma\bar{\Omega}Y_{11}Y_{21} + Y_{12}Y_{21})}{\Gamma}, \quad D_{34} = -\frac{2\zeta\omega_{01}(\gamma\bar{\Omega}Y_{21}^2 + Y_{21}Y_{22})}{\Gamma}\frac{N_1}{N_2},$$

$$D_{43} = \frac{2\zeta\omega_{01}(\gamma\bar{\Omega}Y_{11}^2 + Y_{11}Y_{12})}{\Gamma}\frac{N_2}{N_1}, \quad D_{44} = \frac{2\zeta\omega_{01}(\gamma\bar{\Omega}Y_{11}Y_{21} + Y_{11}Y_{22})}{\Gamma},$$

$$A_{13} = -2\mu\bar{\Omega}\frac{(\gamma^2+\kappa_2)\bar{\Omega}X_{21}Y_{11} + \gamma X_{21}Y_{12}}{\Lambda}, \quad A_{14} = -2\mu\bar{\Omega}\left[\frac{(\gamma^2+\kappa_2)\bar{\Omega}X_{21}Y_{21} + \gamma X_{21}Y_{22}}{\Lambda}\right]\frac{N_1}{N_2},$$

$$A_{23} = 2\mu\bar{\Omega}\left[\frac{(\gamma^2+\kappa_2)\bar{\Omega}X_{11}Y_{11} + \gamma X_{11}Y_{12}}{\Lambda}\right]\frac{N_2}{N_1}, \quad A_{24} = 2\mu\bar{\Omega}\,\frac{(\gamma^2+\kappa_2)\bar{\Omega}X_{11}Y_{21} + \gamma X_{11}Y_{22}}{\Lambda},$$

$$A_{31} = -2\mu\bar{\Omega}\left[\frac{\gamma(\gamma\bar{\Omega}Y_{21}X_{11} - Y_{21}X_{12})}{(1+\delta m)\Gamma} + \frac{\kappa_2\bar{\Omega}Y_{21}X_{11}}{\Gamma}\right],$$

$$A_{32} = -2\mu\bar{\Omega}\left[\frac{\gamma(\gamma\bar{\Omega}Y_{21}X_{21} - Y_{21}X_{22})}{(1+\delta m)\Gamma} + \frac{\kappa_2\bar{\Omega}Y_{21}X_{21}}{\Gamma}\right]\frac{N_1}{N_2},$$

$$A_{41} = 2\mu\bar{\Omega}\left[\frac{\gamma(\gamma\bar{\Omega}Y_{11}X_{11} - Y_{11}X_{12})}{(1+\delta m)\Gamma} + \frac{\kappa_2\bar{\Omega}Y_{11}X_{11}}{\Gamma}\right]\frac{N_2}{N_1},$$

$$A_{42} = 2\mu\bar{\Omega}\left[\frac{\gamma(\gamma\bar{\Omega}Y_{11}X_{21} - Y_{11}X_{22})}{(1+\delta m)\Gamma} + \frac{\kappa_2\bar{\Omega}Y_{11}X_{21}}{\Gamma}\right],$$

$$B_{11} = \mu\frac{\gamma\bar{\Omega}X_{21}X_{11}}{\Lambda}, \quad B_{12} = \mu\frac{\gamma\bar{\Omega}X_{21}^2}{\Lambda}\frac{N_1}{N_2}, \quad B_{21} = -\mu\frac{\gamma\bar{\Omega}X_{11}^2}{\Lambda}\frac{N_2}{N_1}, \quad B_{22} = -\mu\frac{\gamma\bar{\Omega}X_{21}X_{11}}{\Lambda},$$

$$B_{33} = -\mu\frac{\gamma\bar{\Omega}Y_{21}Y_{11}}{\Gamma}, \quad B_{34} = -\mu\frac{\gamma\bar{\Omega}Y_{21}^2}{\Gamma}\frac{N_1}{N_2}, \quad B_{43} = \mu\frac{\gamma\bar{\Omega}Y_{11}^2}{\Gamma}\frac{N_2}{N_1}, \quad B_{44} = \mu\frac{\gamma\bar{\Omega}Y_{21}Y_{11}}{\Gamma},$$

$$\Lambda = X_{11}X_{22} - X_{12}X_{21}, \quad \Gamma = Y_{11}Y_{22} - Y_{12}Y_{21}.$$

References

[1] A. Lawrence, *Modern Inertial Technology, Navigation, Guidance, and Control*, Springer, New York, 1992.
[2] N. Maluf, *An Introduction to Microelectromechanical System Engineering*, Artech House Inc., Boston and London, 2000.
[3] M.W. Putty, K. Najafi, A micro machined vibrating ring gyroscope, *Solid-State Sensor and Actuator Workshop*, Hilton Head, South Carolina, 1994.
[4] S.C. Huang, W. Soedel, Effect of Coriolis acceleration on the free and forced in-plane vibrations of rotating rings on elastic foundation, *Journal of Sound and Vibration* 115 (2) (1987) 253–274.
[5] R. Eley, C.H.J. Fox, S. McWilliam, Coriolis coupling effects on the vibration of rotating rings, *Journal of Sound and Vibration* 238 (3) (2000) 459–480.
[6] D.C. Kammer, A.L. Schlack Jr., Effects of nonconstant spin rate on the vibration of a rotating beam, *Journal of Applied Mechanics* 54 (1987) 305–310.
[7] E. Van Doorn, S.F. Asokanthan, Attitude stability of dual-spin asymmetric spacecraft, *Journal of the Astronautical Sciences* 44 (2) (1996) 149–165.
[8] S. Natsiavas, Non-linear parametric resonance of spinning rings, *Journal of Sound and Vibration* 184 (1) (1995) 93–109.
[9] A.E.H. Love, *Treatise on the Mathematic Theory of Elasticity*, Cambridge, London, 1960.
[10] W. Soedel, *Vibrations of Shells and Plates*, Marcel Dekker, Inc., New York and Basel, 1981.
[11] W.B. Bickford, E.D. Reddy, On the in-plane vibrations of rotating ring, *Journal of Sound and Vibration* 101 (1) (1985) 13–22.
[12] A.L. Nayfeh, *Perturbation Methods*, Wiley, New York, 1973.
[13] N.N. Bogoliubov, Y.A. Mitropolsky, *Asymptotic Methods in the Theory of Non-linear Oscillations*, Hindustan Publishing Corp., Delhi-6, India, 1961.
[14] S.T. Ariaratnam, N. Sri Namachchivaya, Periodically perturbed linear gyroscopic systems, *Journal of Structural Mechanics* 14 (2) (1986) 153–176.